

Noninvasive Sizing of Subcellular Organelles With Light Scattering Spectroscopy

Hui Fang, Mario Ollero, Edward Vitkin, Lauren M. Kimerer, P. B. Cipolloni, Munir M. Zaman, Steven D. Freedman, Irving J. Bigio, Irving Itzkan, Eugene B. Hanlon, and Lev T. Perelman

Abstract—A long-standing impediment for applications of optical techniques in cellular biology is the inability to characterize subcellular structures whose dimensions are much less than about $1\ \mu\text{m}$. In this paper, we describe a method based on light scattering spectroscopy that can find the size distribution of subcellular organelles as small as $100\ \text{nm}$ with an accuracy of $20\ \text{nm}$. We report experiments using aqueous suspensions of subcellular organelles enriched in mitochondria, zymogen granules, and microsomes. From the observed light scattering spectra, we extract size distributions that are in excellent agreement with the results of electron microscopy. Further studies are underway to extract the shapes of organelles in addition to their sizes.

Index Terms—Light scattering spectroscopy (LSS), optical sizing, organelles, scattering, submicrometer.

I. INTRODUCTION

CELLS ARE the fundamental building blocks of organisms. Yet despite significant advances in our knowledge of the molecular basis of cell function and its expression into whole organisms, the most intriguing fact about cells remains our lack of information about their living, internal functioning. The main reason for this gap in modern biology is the absence of a tool that can monitor cells and subcellular organelles at the submicrometer level without disrupting their function. A very important cell biology instrument—the electron microscope—can resolve subcellular structure with very high resolution, but it can only work with nonfunctional

cells [1]. Researchers are studying various modifications of optical microscopy because of the noninvasive nature of visible light [2]. However, because absorption of visible light by cellular structures is very weak, cells routinely require staining to provide optical contrast, and staining may interrupt normal cell function. There are several microscopic techniques which attempt to circumvent this problem by taking advantage of the subtle differences in refractive index between cell structures and their surrounding medium, for example, phase contrast and interference contrast microscopies. However, these techniques only take advantage of changes of the refractive index over a relatively narrow wavelength band and do not utilize internal interference of light. Furthermore, because of diffraction, optical microscopy has difficulty resolving objects smaller than the wavelength of the light used [3]. This constrains the spatial resolution of conventional optical microscopy to approximately $1\ \mu\text{m}$. In this paper, we report observation of subcellular organelles well beyond the diffraction limit and without staining, by utilizing organelle relative refractive index as well as organelle internal light interference. The technique we are using is based on light scattering spectroscopy (LSS). Although LSS has been used to characterize structures larger than a wavelength [4]–[7], in this paper we specifically concentrate on organelles that are smaller than a wavelength, since they represent an important challenge for optical techniques.

Previously, LSS has been used to characterize changes in tissue on the cellular scale and to detect dysplastic changes in epithelial tissues. In 1998, Perelman *et al.* observed characteristic LSS spectral behavior in the light backscattered from nuclei of human intestinal cells [4]. Later these studies were extended to several more organs by Backman *et al.* [5] and Wallace *et al.* [8]. Bigio and Mourant [6] and Mourant *et al.* [9] demonstrated that spectroscopic features of elastically scattered light could be used to detect the transitional carcinoma of the urinary bladder and adenoma and adenocarcinoma of the colon and rectum with good accuracy. Backman *et al.* [10], Sokolov *et al.* [7], and Jacques *et al.* [11] used LSS in combination with polarized light to remove the multiple scattered light and improve the extraction of single-scattered light.

Recently, there has been increased interest in studying subcellular morphology using various light scattering techniques. Mourant *et al.* [12], [13] studied the spectral and angular dependence of light scattering from fibroblast cells. Boustany *et al.* [14] used an optical scattering imaging technique to study morphological changes in functioning cells. Wax *et al.* [15] used angle-resolved low coherence interferometry to study cellular organization in cell monolayers. Backman *et al.* [16] studied

Manuscript received November 15, 2002; revised March 13, 2003. This work was supported by the NSF under Grant BES-0116833, CIMIT New Concepts Award, and OBGYN Foundation, and in part by a Merit Review Grant, Medical Research Service, Department of Veterans Affairs.

H. Fang is with the Department of Obstetrics, Gynecology, and Reproductive Biology and the Department of Medicine, Beth Israel Deaconess Medical Center and Harvard Medical School, Boston, MA 02215 USA, and also with the Physics Department, Boston University, Boston, MA 02215 USA.

M. Ollero, E. Vitkin, M. M. Zaman, S. D. Freedman, I. Itzkan, and L. T. Perelman are with the Department of Obstetrics, Gynecology, and Reproductive Biology and the Department of Medicine, Beth Israel Deaconess Medical Center and Harvard Medical School, Boston, MA 02215 USA (e-mail: ltpere@caregroup.harvard.edu).

L. M. Kimerer and E. B. Hanlon are with the Department of Veterans Affairs, Medical Research Service and Geriatric Research, Education and Clinical Center, Bedford, MA 01730 USA.

P. B. Cipolloni is with the Department of Veterans Affairs, Medical Research Service and Geriatric Research, Education and Clinical Center, Bedford, MA 01730 USA, and also with the Department of Anatomy and Neurophysiology and the Department of Neurology, Boston University School of Medicine, Boston, MA 02215 USA.

I. J. Bigio is with the Department of Biomedical Engineering and the Department of Electrical and Computer Engineering, Boston University, Boston, MA 02215 USA.

Digital Object Identifier 10.1109/JSTQE.2003.812515

light scattering from cells and reported observation of signals from both nuclei and smaller organelles. And Drezek *et al.* investigated the influence of cell morphology on scattering patterns [17].

In this paper, we investigate the ultimate spatial resolution and accuracy of LSS in sizing subcellular organelles and demonstrate that LSS could be a powerful tool to study functioning biological structures down to 100 nm in size.

II. THEORY OF LIGHT SCATTERING BY SUBCELLULAR ORGANELLES

Our goal is to extract information contained in light scattering spectra about the size distribution of small, intracellular organelles. Therefore, we need a model that describes light scattering spectra in terms of organelle physical properties. From the optical point of view, subcellular organelles can be described approximately as spherical particles with refractive indexes n_s slightly different from the refractive index of the surrounding medium n_m . The range of relative refractive indexes for subcellular organelles $m = n_s/n_m$ is 1.03 to 1.06 [18]. In this paper, we use Mie theory to model the scattering spectra of organelles. Mie theory provides an exact analytical solution for the scattering of a plane wave by a sphere; however, it can also provide a first-order description of optical effects in nonspherical particles [19]. Since small organelles in general have spheroidal shape (both prolate and oblate) and since spheroids are randomly oriented in our samples, Mie theory should be a good first-order approximation. Our recent preliminary studies indicate that LSS can sense the shape of organelles as well, and we will publish those results in a subsequent paper on this topic.

Mie theory is an exact solution to the problem. However, it is not easy to recognize which parameters dominate the result. It provides the relative scattering intensity $I_s(\lambda)/I_o(\lambda)$ at the detector in the form of a complex series which depends on a large number of parameters, such as diameter of the scatterer δ , incident wavelength λ , refractive indexes of the scatterer n_s and surrounding medium n_m , scattering angles θ and φ , and polarization state of the incident wave. The intensity is also scaled with a factor L^{-2} where L is the distance from scatterer to detector. All these parameters affect the scattering spectrum, which makes it difficult to extract scatterer size distributions, especially if values for many of the parameters are unknown.

However, since we are interested in the scattering of incoherent, nonpolarized light by organelles, which are smaller than a wavelength, the problem can be significantly simplified. The Rayleigh–Gans approximation [19], which should be quite accurate for small scatterers with relative refractive indexes close to unity gives a good idea about the importance of various parameters. It reveals the fact that the shape of the scattering spectrum $I_s(\lambda)/I_o(\lambda)$ depends strongly on the size parameter $x = (\pi n_m \delta / \lambda)$ and very weakly on the scattering angle θ . It also shows that the amplitude of the scattering spectrum is linearly scaled with $(m-1)^2$ and the scaling factor, which now can be written as δ^2/L^2 . The Rayleigh–Gans approximation yields

$$\frac{I_s}{I_o} \approx \frac{\delta^2}{L^2} (m-1)^2 f\left(x \sin \frac{\theta}{2}\right) \frac{1 + \cos^2 \theta}{(1 - \cos \theta)^2} \quad (1)$$

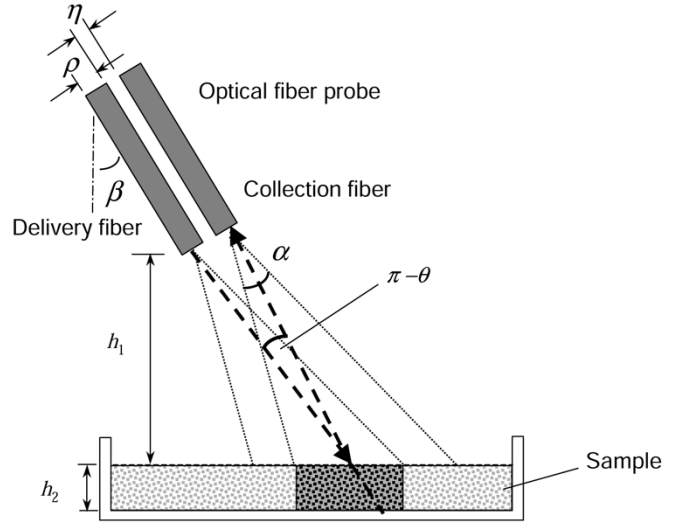


Fig. 1. Schematic diagram of the LSS measurements. Delivery optical fiber (core diameter $\rho = 200 \mu\text{m}$) is located at $h_1 \approx 4 \text{ mm}$ from the sample (sample depth $h_2 \approx 2 \text{ mm}$). Backscattered light (scattering angle $\theta \approx 170^\circ$) is collected by a collection optical fiber separated by $\eta \approx 35 \mu\text{m}$ from the delivery fiber. Angle α is determined by the NA of the fibers. Dark area is an area from which predominately single backscattered light is collected.

where f is a form factor [20]. From (1), it is easy to see that the relative refractive index affects only the magnitude of the scattering intensity but not its shape. Angular effects are even weaker. There is less than 3% change in the scattering intensity for the range of scattering angles from 155° to 180° . For our experimental measurements with a fiber-optic probe (Fig. 1), the range of scattering angles was even narrower. Using simple geometrical considerations, it is easy to see that the backscattering angles are limited by the following expression:

$$\pi - \theta < \frac{(\eta + 2\rho) \cdot \cos(\beta)}{h_1} \quad (2)$$

where η is the separation of the delivery and collection fibers, ρ is fiber core diameter, β is the deviation of the fiber probe from the normal direction, and h_1 is the distance from the tip of the probe to the sample. Using typical numbers of $\eta \approx 35 \mu\text{m}$, $\rho = 200 \mu\text{m}$, $\beta \approx 25^\circ$, and $h_1 \approx 4 \text{ mm}$, we find that the range of backscattering angles is smaller than 5.6° . This angle range results in a 0.3% variation in the scattering intensity.

These analytical results also agree with calculations using the Mie model, for which we adapted the BHMIE code described in [19]. Fig. 2 illustrates the results of these calculations. We used the differential scattering coefficient $p(\theta)Q_{\text{sca}} = I_s(\lambda, \theta)/I_o(\lambda) (4L^2/\pi\delta^2)$, where $p(\theta)$ is scattering phase function, and Q_{sca} is the scattering coefficient, because it is dimensionless and is independent of the distance from scatterer to detector. Also, since the inverse size parameter $1/x$ is linearly proportional to the wavelength, we plotted differential scattering coefficient versus the inverse size parameter in Fig. 2 in order to agree with the usual way of plotting scattering coefficients.

The resulting composite graph represents the differential scattering coefficient for spherical particles over a wide range of parameters. Diameters from 20 to 900 nm and wavelength range

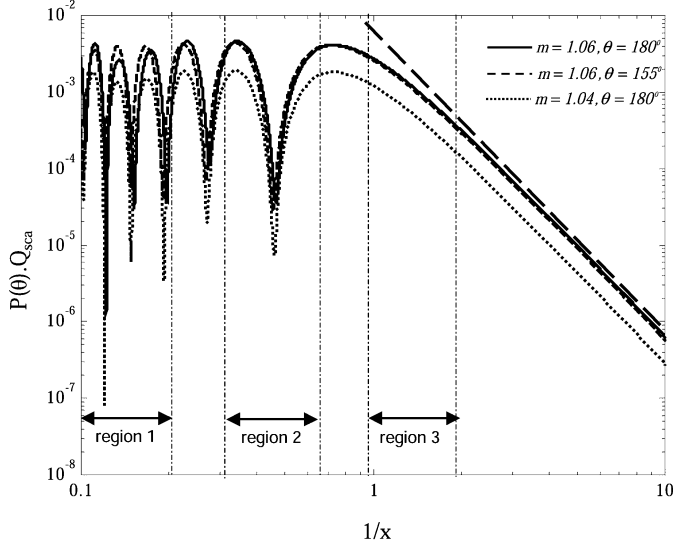


Fig. 2. Composite graph of the differential scattering coefficient for spherical particles in the range of diameters from 20 to 900 nm and the wavelength range from 400 to 800 nm versus inverse size parameter $1/x = \lambda/(\pi n_m d)$. Region 1 shows the behavior of the differential scattering coefficient over the wavelength range from 400 to 800 nm for 900-nm particles. Region 2 and Region 3 show the behavior over the same wavelength range for 300-nm particles and for 100-nm particles, respectively. The three plots represent the following combinations of relative refractive index m and scattering angle θ : $m = 1.06$ and $\theta = 180^\circ$ (solid curve); $m = 1.06$ and $\theta = 155^\circ$ (dashed curve); $m = 1.04$ and $\theta = 180^\circ$ (dotted curve). The straight dashed line is proportional to λ^{-4} and shows the slope of Rayleigh scattering.

from 400 to 800 nm are included. We plotted three spectra for the following relative refractive indexes and scattering angles: $m = 1.06$ and $\theta = 180^\circ$, $m = 1.06$ and $\theta = 155^\circ$, $m = 1.04$ and $\theta = 180^\circ$. The relative refractive indexes are within the range of organelle refractive indexes provided in this section and the scattering angles are within the range limited by the NA of the delivery and collection fibers in the LSS probe (NA = 0.21).

The graph shows that the smallest scatterer size that can be detected reliably without number density information is about 100 nm. For smaller sizes, the spectrum becomes practically indistinguishable from the Rayleigh scattering spectrum, which is proportional to $1/\lambda^4$. For size information in this region, one needs an independent measurement of the number density. It also shows that the effects of scattering angle and refractive index for the spectral range and the range of the particle sizes considered can be neglected. Thus, the only important parameter that affects the LSS spectrum is the size of the scatterer.

III. RECONSTRUCTION OF THE NUMBER DENSITY DISTRIBUTION

The experimentally measured LSS spectrum collected in a particular solid angle is a linear combination of the LSS spectra of subcellular organelles of various types, sizes, and refractive indexes. However, since we are dealing with only relatively small, submicrometer, organelles, the problem is simplified. We can safely assume that the LSS spectrum is independent of relative refractive index m and scattering angle θ and choose values of m and θ within the range described in Section II. Then we

can express the experimental spectrum as an integral only over the organelles' diameters δ

$$S(\lambda) = \int_0^{\delta_{\max}} \tilde{I}(\lambda, \delta) F(\delta) d\delta + \varepsilon(\lambda) \quad (3)$$

where $\tilde{I}(\lambda, \delta) = I_s(\lambda, \delta)/I_0(\lambda)$ is the LSS spectrum of a single scatterer with diameter δ (within the range from 0 to δ_{\max}), $F(\delta)$ is the organelle size distribution, and $\varepsilon(\lambda)$ is the experimental noise.

From Fig. 2, it is easy to see that very small ($\delta_R < 100$ nm) scatterers exhibit Rayleigh behavior proportional to $1/\lambda^4$. In an actual spectrum the origin of the Rayleigh part could come from very small particles present in a cell and also from large protein macromolecules. This Rayleigh contribution should be removed from the spectrum. To do this, we can rewrite (3) as

$$S(\lambda) = \frac{C_R}{\lambda^4} + \int_{\delta_R}^{\delta_{\max}} \tilde{I}(\lambda, \delta) F(\delta) d\delta + \varepsilon(\lambda) \quad (4)$$

where the unknown constant C_R is proportional to the number of Rayleigh scatterers contributing to the total spectrum. To remove the Rayleigh term, we multiply (4) by λ^4 and take a derivative of both sides of the equation

$$\frac{d[S(\lambda) \cdot \lambda^4]}{d\lambda} = \int_{\delta_R}^{\delta_{\max}} \frac{d[\tilde{I}(\lambda, \delta) \cdot \lambda^4]}{d\lambda} F(\delta) d\delta + \frac{d[\varepsilon(\lambda) \cdot \lambda^4]}{d\lambda} \quad (5)$$

Let us introduce the following notation: $\hat{S} = (d[S(\lambda) \cdot \lambda^4]/d\lambda)$, $\hat{I} = (d[\tilde{I}(\lambda, \delta) \cdot \lambda^4]/d\lambda)$ and $\hat{E} = (d[\varepsilon(\lambda) \cdot \lambda^4]/d\lambda)$. Then (5) can be written as a discreet sum over organelles' diameters δ

$$\hat{S}(\lambda) = \sum_{\delta_R}^{\delta_{\max}} \hat{I}(\lambda, \delta) \hat{F}(\delta) + \hat{E}(\lambda) \quad (6)$$

where $\hat{F}(\delta) = F(\delta)d\delta$ is a discreet size distribution. To extract this size distribution, it is convenient to write (6) in matrix form

$$\hat{S} = \hat{I} \cdot \hat{F} + \hat{E}. \quad (7)$$

The dimension p of the vector \hat{S} is determined by the number of spectral points; the dimension q of the vector \hat{F} is determined by the range of the diameters δ_R to δ_{\max} and the size resolution $\Delta\delta$. Thus, the dimension of the matrix \hat{I} is equal to $p \times q$.

Since a certain amount of noise is present in the experimental spectrum \hat{S} , it is not feasible to calculate the size distribution \hat{F} by directly inverting the matrix \hat{I} . Another method that can be used to solve (7) is minimization of the functional

$$\Phi = \sqrt{\sum_{\lambda} (\hat{S} - \hat{I} \cdot \hat{F})^2} \Rightarrow \min \quad (8)$$

where the sum is calculated over all spectral points. However, since the matrix $\hat{I}^T \hat{I}$ is ill-conditioned, (8) constitutes an ill-posed problem [21]–[24]. To solve it, we need to employ additional prior information about the spectrum. For example, researchers previously assumed that the size distribution has a particular known form, such as a single-mode Gaussian distribution [10] or a skewed logarithmic normal distribution

[25]. However, in our case, we are not dealing with a single type of organelle but with a mixture of organelles of different types. Therefore, these single-mode distributions are not sufficient to describe the multimode distribution of sizes due to different types of organelles.

Thus, we do not make any assumptions about the form of the size distribution except that the size distribution cannot be negative

$$\hat{F}(\delta) \geq 0. \quad (9)$$

This is an important constraint, which makes the solution of the problem (8) stable. We then used the linear least squares with nonnegativity constraints algorithm [26], [27] to invert the size distribution.

We can also optimize the dimensions p and q . To do so, we evaluated the amount of information present in the light scattering spectra. The spectroscopic range of our system is from 284 to 831 nm with a resolution of 4 nm. However, since the spectrometer, charged-coupled device (CCD) combination has a low efficiency below 340 nm and there are optical distortions in the system above 780 nm, we chose to use data collected in the range 345 to 745 nm. This constitutes a bandwidth of 400 nm for $p = 100$ independent spectral points. Thus, the highest number of points across the range of sizes should be limited by 100. Since our Mie scattering calculations showed that the LSS spectra of small scatterers are predominantly smooth with only a few sharp spikes, the number of points needed to resolve the sharpest features of the spectra is only about half that number. For the range of sizes from $\delta_R = 100$ nm to $\delta_{\max} = 1000$ nm, we use $q = 45$ which gives a size resolution $\Delta\delta = 20$ nm. The size resolution of $\Delta\delta = 20$ nm is in good agreement with the accuracy of the LSS technique, which we established in the calibration studies with submicrometer polystyrene beads described in Section V.

Because the CCD in our system has 1024 pixels in the spectral dimension or 0.5 nm per pixel, the actual number of the data points from 345 to 745 nm interval is 800. This data is highly redundant since, as we explained above, only 100 spectral points are independent. However, by using all 800 points, we reduce the noise by a factor of $\sqrt{800/100}$ or 2.8 times.

IV. EXPERIMENTAL ARRANGEMENT

LSS spectra were collected using the experimental system described in Fig. 3. A 100-W xenonarc lamp was used as a source of white light. An imaging spectrograph (Acton Research SP-150) and a high efficiency CCD with thermoelectric cooling (Andor Technology DU-434-FI) were employed for light detection in the 290–820-nm wavelength range. The detector was controlled by a computer, into which the data were transferred, stored, and processed. We delivered and collected light using an optical fiber probe, consisting of a central delivery fiber and several rings of collection fibers, with a 200- μm core diameter and an NA = 0.21. The probe was placed 4 mm away from the sample at an approximately 25° angle to prevent specular reflection returning to the collection fibers. The sample consisted of a liquid suspension of either beads or organelles held in a Petri dish. The dish was mounted on a vertical translator which

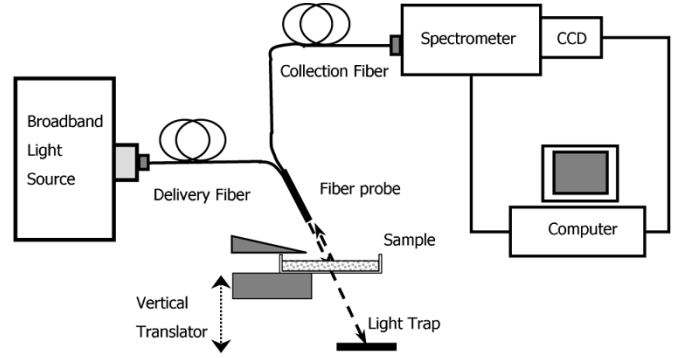


Fig. 3. Schematic diagram of the light scattering spectroscopic experimental system.

was used to adjust the distance between the sample and the fiber probe. Since the sample was mostly transparent, a light trap was placed below the Petri dish.

V. RESULTS

A. Technique Calibration

In order to calibrate the LSS system and to establish the ability of LSS to detect and differentiate submicrometer particles, we performed experiments with polystyrene microspheres with diameters of 175 and 356 nm (Polyscience, Inc.) suspended in water and glycerol.

We first performed measurements on binary mixtures of polystyrene microspheres in water and established that the technique could separate particles of multiple sizes. However, the relative refractive index of the microspheres in water ($n = 1.195$) is substantially higher than that of subcellular organelles in cytoplasm, which is in the range $n = 1.03$ – 1.1 [28]. Therefore, we used glycerol to decrease the relative refractive index of beads to ~ 1.07 – 1.1 in order to better approximate biological conditions. We used the measurements on polystyrene beads in glycerol as a calibration of the technique since the index match is closer to that expected for organelles.

The suspensions were prepared so that the optical thickness τ was 0.2 ($\tau = \mu_s z$, where μ_s is the scattering coefficient and z is the distance into the solution. A photon propagating through a medium with $\tau = 1$ will undergo one scattering event on average.) The refractive index of the beads can be accurately described by the expression [29] $n_s = 1.5607 + 10,002/\lambda^2$ (λ in nanometers). Thus, the relative refractive index of microspheres in glycerol ($n_0 = 1.47$) is $n = 1.071$ – 1.103 leading to realistic relative refractive indexes for subcellular organelles.

The spectra predicted by Mie theory were fitted to the data using least-squares minimization, as described in Section III. The experimental spectra and resulting fits are shown in Fig. 4(a) for microspheres with nominal diameters of 175 and 356 nm. LSS yielded the distributions shown in Fig. 4(b). The peaks of the distributions are 155 and 346 nm. These distributions can be overlaid with Gaussian functions, which yield standard deviations of 27 and 39 nm for the distributions peaked at 155 and 346 nm, respectively. The manufacturer provided specifications for the two sizes of microspheres used as 175 nm with a standard deviation of 10 and 356 nm with a

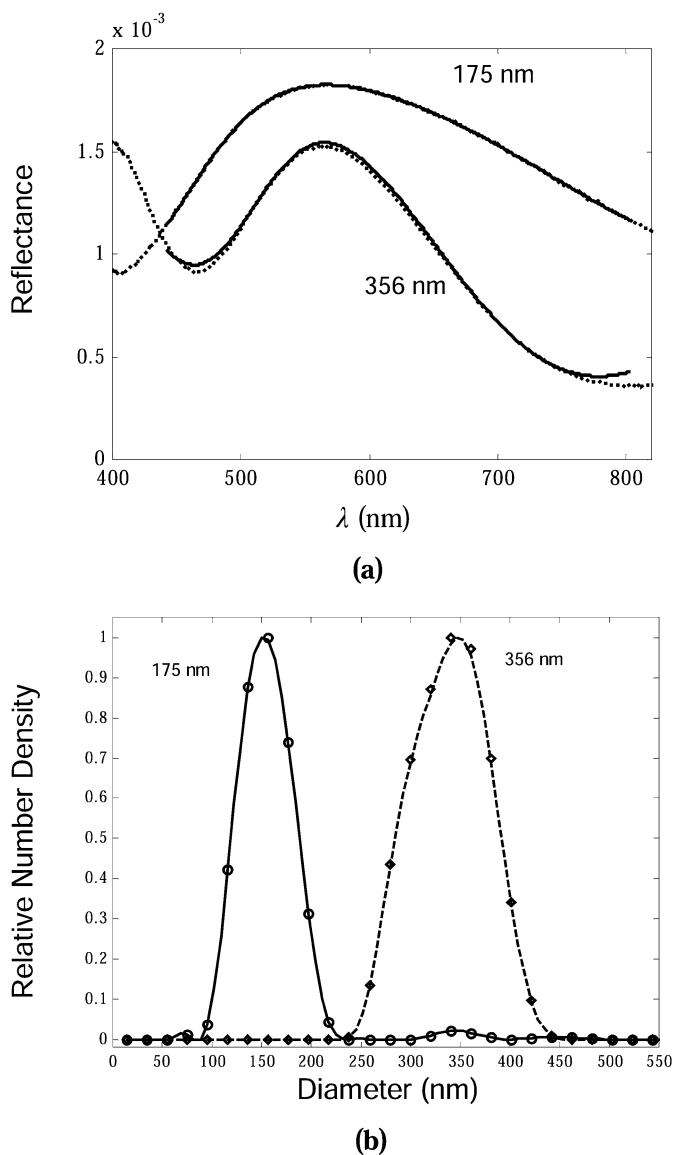


Fig. 4. (a) LSS spectra of light scattered by polystyrene microspheres with nominal diameters of 175 and 356 nm in glycerol. The dotted lines are experimental data and the solid lines are Mie theory predictions. The integration times are 2.5 and 3.75 s, respectively. (b) Size distributions of polystyrene microspheres determined by LSS. The solid line is the LSS determined distribution for the 175-nm microsphere sample and the dashed line is the LSS determined distribution for the 356-nm microsphere sample (circles and diamonds are the actual reconstructed data points).

standard deviation of 14 nm, which is in good agreement with our reconstructed distributions. (The manufacturer does not provide the functional form of the size distributions for either size of microspheres.) Based on these numbers, the accuracy of the LSS method is estimated to be 20 nm.

B. Cell Subfractionation

We then performed LSS experiments with suspensions of nuclei, mitochondria, zymogen granules, and microsomes extracted from cells by means of differential centrifugation. Differential centrifugation is the most common technique for the separation of cells and subcellular fractions, and is a routine method in biomedical laboratories. Separation takes place as a

function of the difference in the terminal velocities of different particles, as determined by Stoke's law

$$v_t = \frac{\delta^2(p_s - p_m)a}{(18\mu)} \quad (10)$$

where v_t is the terminal velocity of the particle, δ the diameter of the particle, a the centrifugal acceleration, μ the viscosity of the medium, p_s the density of the particle, and p_m the density of the medium. Each fraction obtained through differential centrifugation contains a few different types of organelles, which have similar sedimentation velocities, i.e., similar values of $\delta^2(p_s - p_m)/4$. Further separation can be achieved by centrifugation on density gradients or by more complex technologies.

Pancreatic exocrine acinar cells represent a suitable cell type for the study of subcellular fractions, due to their availability and to the presence of a unique subcellular structure, the secretory zymogen granules (secretory vesicles containing inactive precursors of pancreatic enzymes). This makes it the cell type of choice for the study of the events involved in the synthesis and secretion of proteins.

Zymogen granules have variable sizes, with a maximum diameter of 1.3 μm . The rest of organelles include mitochondria, variable in size and shape, ranging between 0.2 and 1 μm ; and ribosomes, small opaque particles of 15 nm in diameter, present in membranous structures (rough endoplasmic reticulum or microsomes) [30].

In the present study, pancreatic acinar cells from rats were subfractionated by differential centrifugation, following a protocol based on the method described in 1967 by Jamieson and Palade [31] for the same cell type in guinea pigs. Briefly, adult rats were sacrificed by asphyxiation and pancreatectomized. Pancreas was minced with scissors, suspended in 8 mL of 0.3-M sucrose and placed in a Dounce homogenizer on ice. Homogenized tissue was transferred to centrifuge tubes and centrifuged at 600 g for 10 min in an International Equipment Company (IEC) clinical centrifuge. The supernatant was transferred to a clean tube and centrifuged at 1000 g for 10 min. The pellet was resuspended in 4 mL of 0.3 M sucrose and labeled as "Fraction 1." The supernatant was transferred to a clean tube and centrifuged at 8700 g for 15 min in a Beckman-Coulter Avanti J-25 centrifuge. The pellet was resuspended in 4 mL of 0.3-M sucrose and labeled as "Fraction 2." The supernatant was labeled as "Fraction 3."

C. Electron Microscopy

Size distributions determined by the LSS method were compared with those determined by electron microscopy. The 0.3-mL aliquots of each fraction were transferred to 0.5-mL BEEM capsules. These capsules were used for centrifuging, processing, and embedding, thus leaving the pellets undisturbed throughout the procedure.

After centrifuging at 14 000 rpm for 5 min, the supernatant was discarded and the pellet was resuspended in 0.3 mL of fixative (2% paraformaldehyde and 1% glutaraldehyde in 0.1 M phosphate buffer). The centrifugation step was repeated and the supernatant was replaced by fresh fixative. The fractions were

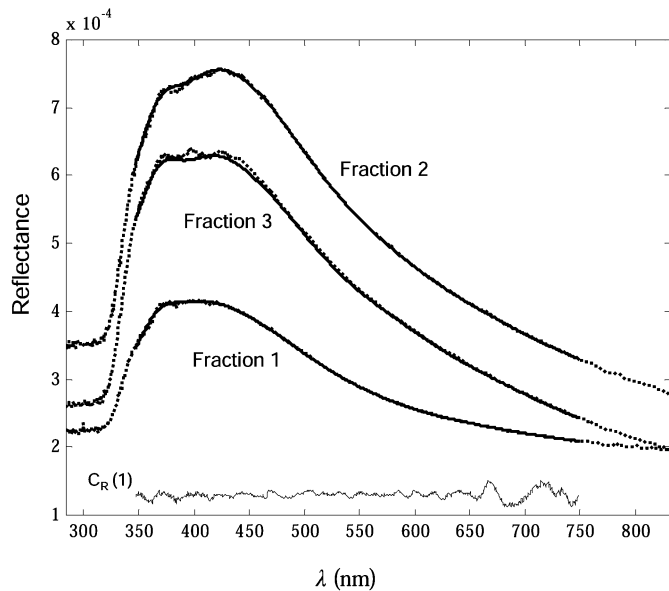


Fig. 5. LSS spectra of light scattered by subcellular organelles in Fractions 1 through 3. The experimental data (dotted lines) and the Mie theory fits (solid lines) are shown. Experimental data is fitted in the 345–745-nm spectral region. The relative reconstruction errors for Fractions 1, 2, and 3 are 0.28%, 0.25%, and 0.48%, respectively. The integration times are 150, 100, and 125 s, respectively. A plot of reconstructed C_R versus wavelength for Fraction 1 shows that the reconstructed C_R is essentially independent of wavelength.

stored overnight at 4 °C, then rinsed and postfixed in cold 1% osmium tetroxide in phosphate buffer. After buffer rinses and poststaining with alcoholic uranyl acetate, the pellets were dehydrated through an ascending series of ethanol concentrations, followed by propylene oxide, followed by a 50/50 mixture of propylene oxide/Epon Araldite resin and an overnight infiltration in 100% Epon Araldite. The pellets were embedded in fresh Epon Araldite the following day and cured in a 60° oven for 48 h.

The resulting blocks containing the pelleted fractions were sectioned using an RMC MT 7000 Ultramicrotome. Semithin (1 μm) sections cut with a glass knife were collected, stained, and examined with the light microscope. At this point, the fixation and curing of the fractions was evaluated and the block was trimmed to encompass the tissue for thin sectioning. The orientation chosen for sampling the cell fractions was normal to the gradient that resulted from centrifuging. The tissue was sampled at increasing depths from the tip of the capsule. At each depth, thin sections were cut with a diamond knife to a thickness corresponding to reference interference colors between silver and gold (approximately 60–80 nm). The sections were placed on formvar-coated copper slot grids and examined and photographed with a Phillips 200 electron microscope at both low and high magnification. The initial perusal of the sections at low power was to confirm the homogeneity of the fraction. In cases where there were particles of varying sizes present, all were photographed.

D. Comparison of LSS With Electron Microscopy

Using the reconstruction technique described in Section III, we found size distributions of organelles in Fractions 1 through

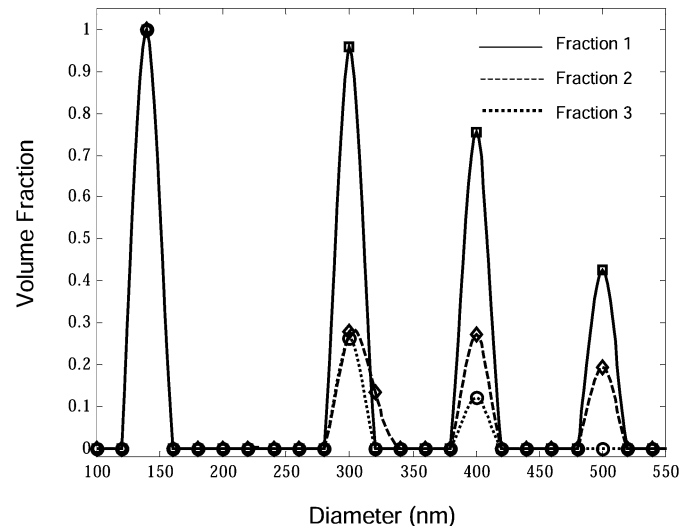


Fig. 6. Organelle volume fractions reconstructed from the spectra presented in Fig. 5. Volume fraction is the organelle number density multiplied by the corresponding organelle volume and normalized to unity. Fraction 1—solid line. Fraction 2—dashed line. Fraction 3—dotted line. (Circles, squares, and diamonds are the actual reconstructed data points).

3. The experimental and reconstructed spectra from these fractions are presented in Fig. 5. The fits of the reconstructed spectra are excellent; the relative difference (defined as $\sqrt{\sum_{\lambda} [S_r(\lambda) - S_e(\lambda)]^2} / \sqrt{\sum_{\lambda} S_e^2(\lambda)}$, where S_e stands for the experiment data and S_r stands for the reconstruction) for Fractions 1, 2, and 3 is 0.28%, 0.25%, and 0.48%, respectively. These values are close to the noise level, which is less than 0.5%.

The corresponding size distributions are presented in Fig. 6. In each of the three fractions, the total number of smaller particles is significantly higher than that for larger particles. To be able to present size distributions on a single graph, we plotted normalized volume fractions of organelles. Volume fraction is defined as organelle number density multiplied by the corresponding organelle volume.

We compared the extracted size distribution for Fraction 3 with morphometry performed on the same fraction using electron micrographs taken at 45 750 magnification, as described in Section V-C. The result is presented in Fig. 7. The morphometric measurements were performed by overlaying the electron microscope photograph with a 100-nm step grid and counting particles of various sizes. We estimate the accuracy of the morphometric sizing to be approximately 20 nm. Morphometry was not performed in two small areas in the upper left and upper right corners of the micrograph (marked in darker shades on Fig. 8) because of the lack of contrast in those areas. For nonspherical particles, we used a mean diameter as the diameter presented in Fig. 7. The size distribution of organelles predicted by the LSS technique (Fig. 7) is in excellent quantitative agreement with the distribution measured using the electron micrograph for 140-, 300-, and 400-nm particles.

It should be pointed out that the electron micrographs provided thin section results since the thickness of the electron microscopy sample (60–80 nm) is smaller than the size of the particles being measured, whereas the LSS sample is very

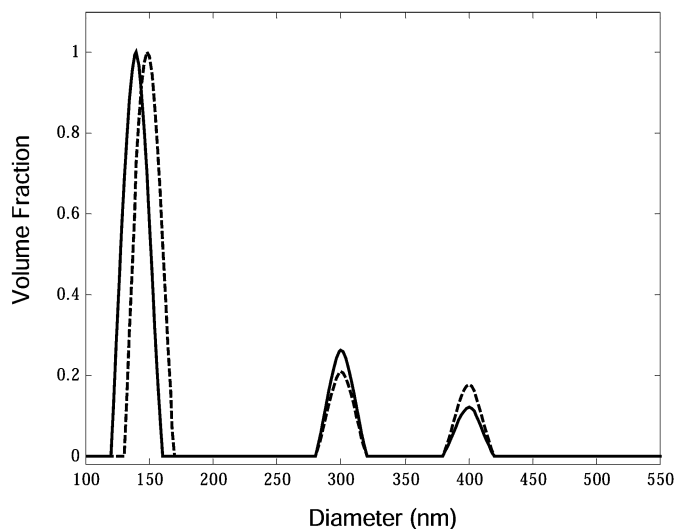


Fig. 7. Comparison of the size distributions of organelles in Fraction 3. The solid line is the distribution extracted from the LSS spectrum and the dashed line is the distribution measured using electron microscopy.

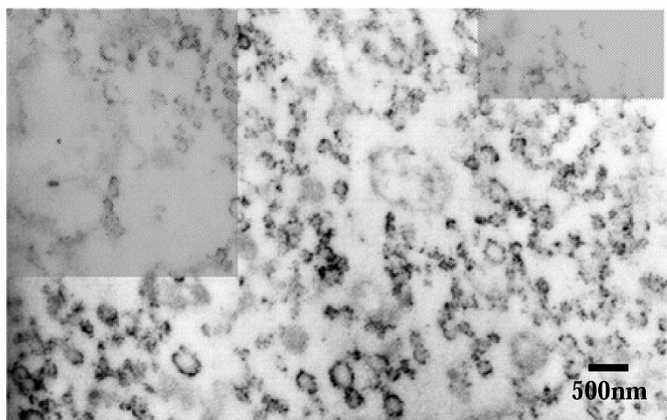


Fig. 8. Electron microscope photograph of Fraction 3 taken with a magnification of 45 750. Solid bar equals 500 nm. The organelles were counted in the bright area of the photograph.

thick ($2 \cdot 10^6$ nm) compared with the particle sizes. To compare electron microscopy results to LSS results, we remapped the two-dimensional (2-D) size distribution determined by morphometry of the electron micrograph thin sections to a three-dimensional distribution by scaling the 2-D number density by the power $3/2$, which takes into account the frequency of appearance of particles of different sizes in the thin sections.

Fraction 3 (Figs. 6 and 8) contains a large number of small organelles along with a small number of larger organelles. The electron microscopy measurements become inaccurate for the relatively few, large (>550 nm) particle sizes present in Fraction 3 because of two reasons. First, the electron microscope samples a very small volume compared with LSS, so larger particles can easily be underrepresented because of poor sampling statistics. Second, the thickness of the electron microscopy sections is much less than the diameter of the large particles. Therefore, for large particles, the diameter of the cross sections in the electron micrograph may not represent the actual diameter of the particle. This results in size distributions that are broadened and mean sizes that are underestimated for large particles.

Therefore, electron microscopy methods we used to confirm organelle size distributions are not applicable to sizes much larger than the thickness of the electron microscopy section.

With the LSS technique described here, we were able to reconstruct organelle size distributions up to $1 \mu\text{m}$. We believe that the LSS accuracy for large particles should be comparable to that shown for small particles in Fig. 7. This is reasonable given our previous results on polystyrene beads and cell nuclei [4], [5]. In this paper, we only present results for particles smaller than 550 nm since we have no independent means of verifying large particle data. Furthermore, the main point of the study was to demonstrate that LSS can be used to measure subcellular organelles with sizes much smaller than an optical wavelength.

The LSS data collection time for these experiments is approximately 2 min per fraction; postexperiment data processing to extract size distributions and refractive indexes takes several seconds. This is significantly faster than electron microscopy, where actual measurements with preprocessing and postprocessing are quite lengthy (hours to days).

VI. DISCUSSION

Previous studies have shown that LSS can provide accurate diffraction-limited detection of cells and cell nuclei [18]. The studies reported here demonstrate that LSS can detect and characterize subcellular organelles whose sizes are at or well below the diffraction limit for optical imaging, down to about 140 nm. Equally important is the accuracy demonstrated in characterizing submicrometer size distributions to within approximately 20 nm. In addition, since it should be possible to reduce the combined data collection and processing time from the minutes reported here to less than 1 s, the method has potential to be a real time technique important for monitoring cellular function. Other advantages of LSS are that the technique is noninvasive and nondestructive.

When applied to polystyrene microspheres, this technique provides size and refractive index information confirmed by manufacturer's specifications. Applied to biological systems, the size distributions determined by LSS for subcellular organelles in centrifugation fractions of cell lysates show excellent agreement with the distributions determined by electron microscopy for organelle sizes less than 550 nm. Furthermore, these distributions show very characteristic widths and specific mean diameters, indicating specific types of organelle are being differentiated. For example, Fig. 6 clearly shows a dominant peak at 140 nm characteristic of smooth-surface microsomes [31]—small round particles clearly visible on the electron micrograph. The three peaks in 300–500-nm region are probably rough-surface microsomes, mitochondria, and zymogen granules of several sizes.

The centrifugation procedure creates fractions enriched in a predominant structure in addition to a mixture of other particles. As we go from Fraction 1 to Fraction 3, we can see this progression. Fraction 1 was enriched in zymogen granules and Fig. 6 shows a large number of 500-nm particles. The main component of Fraction 2 was mitochondria and Fig. 6 shows that many of the larger particles have been removed. Fraction 3 mostly contained both rough (ribosome containing) and smooth (non-ribo-

some containing) microsomes (endoplasmic reticulum derived vesicles), as well as membrane fragments. The distribution of sizes for Fraction 3 is shown in Fig. 7 and analyzed in detail in Section V-D.

Fig. 6 also confirms that for the cell type we used, rat pancreatic exocrine acinar cells, smaller organelles, such as smooth-surface and rough-surface microsomes and mitochondria (up to 500 nm in size) have narrow and well-defined distributions.

In order to evaluate the accuracy of the size distribution reconstruction technique, we compared results of the reconstruction with either measurements based on electron microscopy (for the organelles) or data provided by the manufacturer (for polystyrene beads). However, electron microscopy measurements are limited to a small, thin section of the sample and the manufacturer's information was limited to average size and standard deviation. When such confirmatory information is not available, it would be important to supplement the reconstruction algorithm with an independent technique for evaluating its accuracy. One possible method is a numerical simulation of the experimental spectra, including noise, followed by a statistical analysis of the reconstructed results. This analysis will be reported in a future publication.

Clearly, the ability to extract information about such physical properties as the size and shape of scattering particles depends in part on the optical properties of their surrounding medium. The results of Section II show that for particles smaller than 1 μm , light scattering spectra depend on scatterer size and refractive index. What is important is that these two parameters affect the spectra distinctly. The refractive index of the scatterer weakly affects the shape of the spectrum but significantly affects its magnitude. Therefore, we can be sure that organelle sizes can be extracted accurately, even though relative refractive indexes are not known precisely. Also, if an independent measurement of organelle size or concentration is available, LSS can accurately measure organelle refractive indexes. Nonetheless, since the refractive indexes of subcellular organelles are within a known narrow range, the technique still can give a good estimate for the total number of organelles. In the studies reported here, subcellular organelles were suspended in an aqueous sucrose medium whose refractive index is precisely determined. This may not be the case in studies using intact cells or cell populations. However, to the extent that the cytoplasm is predominantly aqueous, and to the extent that studies as reported here can be used to determine effective refractive indexes of the organelles themselves, the feasibility of LSS measurements on the organelles contained in intact, viable cells, is clear.

LSS monitoring of organelles requires no exogenous labels that might alter organelle function in viable cells. This, combined with the demonstrated specificity and sensitivity to differentiate individual types of organelle noninvasively and in real time, should enable direct monitoring of normal organelle function, as well as organelle functional response to chemically or genetically induced cell signaling processes in functioning cells. Such studies could provide direct information about how the cell responds to the effects of drugs or about important cell cycle processes such as differentiation and apoptosis. Currently, such information must be inferred from studies of nonfunctional or artificially labeled cells.

VII. CONCLUSION

The technique we developed is capable of sizing subcellular organelles in real time without destroying viability. It has the potential for noninvasive monitoring of intact cells, which could be very important for such applications as studying the effects of various agents on cell function. For example, using this technique one can continuously and noninvasively monitor cells and observe effects of various drugs, study apoptosis, etc.

In the present study, we extracted the mean size of the organelles. The ability to identify specific types of subcellular organelles by their LSS spectra, and hence the ability to monitor specific, viable functioning, will be enhanced by the ability to extract shape information in addition to the size information demonstrated here. Our recent studies show that LSS has a capability of extracting shape information. We are currently working on including the shape of the organelles in the technique and will report those results shortly.

ACKNOWLEDGMENT

The electron microscopy studies were conducted at the electron microscope facility, Medical Research Service, Department of Veterans Affairs, Bedford, MA.

REFERENCES

- [1] S. Amelinckx, D. V. Dyck, J. V. Landuyt, and G. V. Tendeloo, Eds., *Electron Microscopy: Principles and Fundamentals*. New York: Wiley, 1997.
- [2] A. J. Lacey, Ed., *Light Microscopy in Biology*. London, U.K.: IRL Press at Oxford Univ. Press, 1989.
- [3] M. Born and E. Wolf, *Principles of Optics*. Cambridge, U.K.: Cambridge Univ. Press, 1999.
- [4] L. T. Perelman *et al.*, "Observation of periodic fine structure in reflectance from biological tissue: A new technique for measuring nuclear size distribution," *Phys. Rev. Lett.*, vol. 80, pp. 627–630, 1998.
- [5] V. Backman *et al.*, "Detection of preinvasive cancer in situ," *Nature*, vol. 406, pp. 35–36, 2000.
- [6] I. J. Bigio and J. R. Mourant, "Ultraviolet and visible spectroscopies for tissue diagnostics: Fluorescence spectroscopy and elastic-scattering spectroscopy," *Phys. Med. Biol.*, vol. 42, pp. 803–814, 1997.
- [7] K. Sokolov, R. Drezek, K. Gossage, and R. Richards-Kortum, "Reflectance spectroscopy with polarized light: Is it sensitive to cellular and nuclear morphology," *Opt. Expr.*, vol. 5, pp. 302–317, 1999.
- [8] M. Wallace *et al.*, "Endoscopic detection of dysplasia in patients with Barrett's esophagus using light scattering spectroscopy," *Gastroenterology*, vol. 119, pp. 677–682, 2000.
- [9] J. R. Mourant *et al.*, "Detection of gastrointestinal cancer by elastic scattering and absorption spectroscopies with the los alamos optical biopsy system," *Proc. SPIE*, vol. 2387, pp. 210–217, 1995.
- [10] V. Backman, R. Gurjar, K. Badizadegan, R. Dasari, I. Itzkan, L. T. Perelman, and M. S. Feld, "Polarized light scattering spectroscopy for quantitative measurement of epithelial cellular structures in situ," *IEEE J. Select. Topics Quantum Electron.*, vol. 5, pp. 1019–1027, July/Aug. 1999.
- [11] S. L. Jacques, J. R. Roman, and K. Lee, "Imaging superficial tissues with polarized light," *Lasers Surg. Med.*, vol. 26, pp. 119–129, 2000.
- [12] J. R. Mourant *et al.*, "Light scattering from cells: The contribution of nucleus and the effects of proliferate status," *J. Biomed. Opt.*, vol. 5, pp. 131–137, 2000.
- [13] J. R. Mourant, T. M. Johnson, and J. P. Freyer, "Characterizing mammalian cells and cell phantoms by polarized backscattering fiber-optic measurements," *Appl. Opt.*, vol. 40, pp. 5114–5123, 2001.
- [14] N. N. Boustany, S. C. Kuo, and N. V. Thakor, "Optical scatter imaging: Subcellular morphometry in situ with fourier filtering," *Opt. Lett.*, vol. 26, pp. 1063–1065, 2001.

- [15] A. Wax, C. Yang, V. Backman, K. Badizadegan, C. W. Boone, R. R. Dasari, and M. S. Feld, "Cellular organization and substructure measured using angle-resolved low-coherence interferometry," *Biophys. J.*, vol. 82, pp. 2256–2264, 2002.
- [16] V. Backman *et al.*, "Measuring cellular structure at submicrometer scale with light scattering spectroscopy," *IEEE J. Select. Topics Quantum Electron.*, vol. 7, pp. 887–893, Nov./Dec. 2001.
- [17] R. Drezek, A. Dunn, and R. Richards-Kortum, "Light scattering from cells: Finite-difference time-domain simulations and goniometric measurements," *Appl. Opt.*, vol. 38, pp. 3651–3661, 1999.
- [18] L. T. Perelman and V. Backman, "Light scattering spectroscopy of epithelial tissues: Principles and applications," in *Handbook on Optical Biomedical Diagnostics*, V. Tuchin, Ed. Bellingham, WA: SPIE, 2002, ch. XII, pp. 675–724.
- [19] C. F. Bohren and D. R. Huffman, *Absorption and Scattering of Light by Small Particles*. New York: Wiley, 1983.
- [20] R. Graaff, J. G. Aarnoudse, J. R. Zijp, P. M. A. Slood, F. F. M. de Mul, J. Greve, and M. H. Koelink, "Reduced light-scattering properties for mixtures of spherical particles: A simple approximation derived from Mie calculations," *Appl. Opt.*, vol. 31, pp. 1370–1376, 1992.
- [21] S. Towmey and H. B. Howell, "Some aspects of the optical estimation of microstructure in fog and cloud," *Appl. Opt.*, vol. 6, pp. 2125–2131, 1967.
- [22] S. Towmey, "Information content in remote sensing," *Appl. Opt.*, vol. 13, pp. 942–945, 1974.
- [23] M. R. Jones, B. P. Curry, M. Q. Brewster, and K. H. Leong, "Inversion of light-scattering measurements for particle size and optical constants: Theoretical study," *Appl. Opt.*, vol. 33, pp. 4025–4034, 1994.
- [24] A. Ben-David and B. M. Herman, "Method for determining particle size distributions by nonlinear inversion of backscattered radiation," *Appl. Opt.*, vol. 24, pp. 1037–1042, 1985.
- [25] J. M. Schmitt and G. Kumar, "Optical scattering properties of soft tissue: A discrete particle model," *Appl. Opt.*, vol. 37, pp. 2788–2796, 1998.
- [26] I. J. D. Craig and J. C. Brown, *Inverse Problems in Astronomy: A Guide to Inversion Strategies for Remotely Sensed Data*. A. Hilger, 1986.
- [27] C. Lawson and R. Hanson, *Solving Least Squares Problems*. Englewood Cliffs, NJ: Prentice-Hall, 1974.
- [28] B. Beauvoit, T. Kitai, and B. Chance, "Contribution of the mitochondrial compartment to the optical properties of rat liver: A theoretical and practical approach," *Biophys. J.*, vol. 67, pp. 2501–2510, 1994.
- [29] E. Marx and G. W. Mulholland, "Size and refractive index determination of single polystyrene spheres," *J. Res. Natl. Bur. Stand.*, vol. 88, pp. 321–338, 1983.
- [30] L. H. Hermodsson, *The Ultrastructure of Exocrine Pancreas Cells as Related to Secretory Activity*. Uppsala: Almqvist & Wiksells, 1965.
- [31] J. D. Jamieson and G. E. Palade, "Intracellular transport of secretory proteins in the pancreatic exocrine cell," *J. Cell Biol.*, vol. 34, pp. 577–596, 1967.



Mario Ollero received the Veterinary Medicine degree, in 1992 and the Ph.D. degree in biochemistry, in 1996, from the University of Zaragoza, Spain.

He was recently appointed Assistant Professor of Obstetrics, Gynecology, and Reproductive Biology, as well as Instructor in Medicine at Harvard Medical School, Boston, MA. He has focused most of his research on the applications of liquid chromatography to the separation of cells based on surface properties and the role of fatty acids in animal and human reproduction. He is currently interested in those aspects of lipid biochemistry involved in the pathogenesis of cystic fibrosis and other genetic and metabolic disorders.

Dr. Ollero has been cofounder of the Spanish Society of Developmental Biology and member of the Spanish Society of Biochemistry, the American Society of Andrology, the American Oil Chemists Society, the European Federation for the Science of Lipids, and the International Society for the Study of Fatty Acids and Lipids.



Edward Vitkin received the M.S. degree from Belarus State University, in 1961 and the Ph.D. degree from the Institute of Physics Academy of Sciences in Minsk, in 1968.

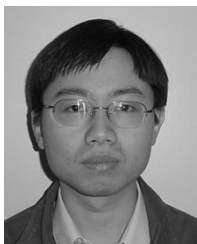
He was Leading Research Scientist at the Laboratory of Optics of Nonequilibrium Media at the Institute of Physics Academy of Sciences until 2001, working on gas dynamics spectroscopy of jet plumes. He is now a Visiting Scientist at Harvard Medical School and Research Scientist at Biomedical Imaging and Spectroscopy Laboratory

at Beth Israel Deaconess Medical Center, Boston, MA. His current area of interests includes light transport in biological tissue and applications to cell biology.



Lauren M. Kimerer received the B.S. degree in biology from Washington College, Chestertown, MD.

She has done electron microscopy research at Case Western University, Cleveland, OH, The Eye Research Institute, Boston, MA, and Boston University School of Medicine, Department of Anatomy, Boston. She is presently the Electron Microscopist at the Electron Microscope Core Facility in the Department of Veterans Affairs Medical Research Service at Bedford, MA, and a member of the Geriatric Research Education and Clinical Center.



Hui Fang received the B.S. and M.S. degrees in optical physics from the University of Science and Technology of China (USTC), Hefei, China, in 1994 and 1997, respectively. He is currently pursuing the Ph.D. degree in biophysics at Boston University, Boston, MA.

From 1997 to 2000, he was with Institute of Modern Optics of Nankai University, Tianjin, China, where he was involved in several projects on white light digital information processing. In 2002, he joined the Biomedical Imaging and Spectroscopy

Laboratory directed by Dr. Perelman at Harvard Medical School and Beth Israel Deaconess Medical Center, Boston, MA, to perform his doctoral research. His interests include the application of light scattering spectroscopy and imaging techniques in the fields of biology and medicine.



P. B. Cipolloni received the M.D. degree from West Virginia University School of Medicine, in 1966 and fulfilled his residency training at Massachusetts General Hospital.

He was a Postdoctoral Fellow, from 1975 to 1979, at Boston University School of Medicine, Boston, MA, where he presently holds appointments in the Department of Anatomy and Neurophysiology and in the Department of Neurology. He is a physician at the ENRM VA Medical Center in Bedford, MA, and a member of the Geriatric Research Education and

Clinical Center. His primary research interest is in cerebral cortical connectivity and cellular organization.



Munir M. Zaman graduated from Dhaka Medical College, Bangladesh, in 1992.

He has focused his research on understanding the role of CFTR gene mutations in chronic inflammatory disorders such as cystic fibrosis, chronic pancreatitis, and primary sclerosing cholangitis. As a Research Fellow at Beth Israel Deaconess Medical Center, Boston, MA, he has created a novel mouse model of bile duct injury by inducing colitis in homozygous and heterozygous CF knockout mice. He has also shown enhanced proinflammatory cytokine secretion from cystic fibrosis monocytes, trying to understand the intracellular signal transduction mechanisms behind this phenomenon.

Dr. Zaman is a Member of the American Gastroenterology Association.



Steven D. Freedman received the B.A. degree from Boston University, Boston, MA, in 1976, the Ph.D. degree in Cell Biology from Yale University School of Medicine, New Haven, CT, in 1981, and the M.D. degree from the University of Connecticut, Storrs, in 1986.

He has focused both his clinical and research career on understanding the pathophysiology of chronic pancreatitis and cystic fibrosis (CF). As a Gastroenterologist at Beth Israel Deaconess Medical Center in Boston, MA, and an Associate Professor at Harvard Medical School, his group has discovered that a fatty acid defect is associated with mutations of the CF gene in both CF knockout mice and humans with the disease. Correction of this defect in this transgenic mouse model reverses the pathology in CF-affected organs. His group has also identified an association between CF gene mutations and chronic pancreatitis as well as primary sclerosing cholangitis.



Irving J. Bigio received the Ph.D. degree in physics from the University of Michigan, Ann Arbor, in 1974.

From 1974 to 2000, he was a Scientific Staff Member at Los Alamos National Laboratory, including service as Group Leader for Laser Science and Applications. He has been a visiting faculty member at the Weizmann Institute of Science, in Israel, the University of Copenhagen, Denmark, and the University of Oxford, England. Since 1986, he has focused his research on biomedical applications of lasers and optics. Since February 2001, he has

been a Professor at Boston University in the Departments of Biomedical Engineering and Electrical & Computer Engineering.

Dr. Bigio holds several patents in biomedical optics, and has received three R&D-100 Awards. He is a Fellow of the Optical Society of America, the American Institute of Medical and Biological Engineering, and the American Society for Laser Medicine & Surgery, and is a Member of the American Physical Society and the SPIE.



Irving Itzkan received the Bachelor degree in engineering physics from Cornell University, Ithaca, NY, in 1952, the Master degree in electrical engineering from Columbia University, New York, in 1961, and the Ph.D. degree in physics from New York University, New York, in 1969.

He is currently a Visiting Scientist at Harvard Medical School and the Biomedical Imaging and Spectroscopy Laboratory, BIDMC, Boston, MA. Prior to that, he was a Senior Scientist in the Massachusetts Institute of Technology Laser Biomedical Research Center, from 1988 to 2000, where his principal research interest was using optical spectroscopy to diagnose disease. From 1956 to 1969, he was with Sperry Rand, and from 1969 to 1985, with the Avco-Everett Research Laboratory where he worked on many different aspects of laser research. His present research interests involves application of optics to cell biology.



Eugene B. Hanlon received the Ph.D. degree in physical chemistry from Boston University, Boston, MA, for studies into the optical and magnetic resonance spectroscopy of molecules in the interfacial state.

He continued postdoctoral studies at Boston University investigating spectroscopic methods for characterizing tissue and laser tissue interactions and developed photoacoustic spectroscopy for monitoring tissue ablation at Summit Technology, Inc. He has served as a consultant in Raman spectroscopy for commercial concerns in medical and nonmedical applications. As a Research Scientist with the National Institutes of Health Laser Biomedical Research Resource at Massachusetts Institute of Technology, Cambridge, he began studies into the spectroscopic diagnosis of Alzheimerts disease and currently heads the program in optical spectroscopy of neurodegenerative disorders at the Department of Veterans Affairs Medical Research Service, Bedford, MA. His current research interests are in the area of laser and molecular spectroscopy applications in clinical medicine and medical research.

Dr. Hanlon was a Zenith Award investigator, Alzheimer's Disease and Related Disorders Association, and is a member of the Optical Society of America and a past Member of the American Chemical Society.



Lev T. Perelman received the Ph.D. degree in physics from the Institute of Physics Academy of Sciences in Minsk, in 1989.

He is currently an Associate Professor at Harvard University and Director of the Biomedical Imaging and Spectroscopy Laboratory at Beth Israel Deaconess Medical Center, Boston, MA. Previously, he was a Principal Research Scientist at the Massachusetts Institute of Technology Laser Biomedical Research Center where his research interest was using optical spectroscopy to diagnose disease. He conceived and developed biomedical light scattering spectroscopy (LSS) recently applied for noninvasive detection of early precancerous changes in epithelial tissues and tissue characterization on subcellular scale. His present research interest involves application of optics to cell biology and detection of disease.